Green Chemistry

PAPER

View Article Online
View Journal | View Issue

Cite this: *Green Chem.*, 2015, **17**, 4830

Assay for lignin breakdown based on lignin films: insights into the Fenton reaction with insoluble lignin†

Michael S. Kent,*[a,b] Isaac C. Avina,[b] Nadeya Rader,[b] Michael L. Busse,[b] Anthe George,[a,b] Noppadon Sathitsuksanoh,[a] Edward Baidoo,[a] Jerilyn Timlin,[b] Nicholas H. Giron,[b] Mathias C. Celina,[b] Laura E. Martin,[b] Ronen Polsky,[b] Victor H. Chavez,[b] Dale L. Huber,[b] Jay D. Keasling,[a,c] Seema Singh,[a,b] Blake A. Simmons[a,b] and Kenneth L. Sale[a,b]

Received 22nd May 2015,
Accepted 30th July 2015

DOI: 10.1039/c5gc01083g

www.rsc.org/greenchem

We report a new assay for breakdown of high molecular weight, insoluble lignin based on lignin films. In this method, decrease in film thickness is detected upon solubilization of mass through either chemical alteration of the lignin or molecular weight reduction. The assay was performed with organosolv lignin, the only chemical modification being an oxidative pretreatment to provide film stability with respect to dissolution. The assay is sensitive to release of as little as 20 Å of material from the film. A multiplexed format was developed using a silicone block in the form of a standard 96-well plate, allowing simultaneous assaying of a large number of reaction conditions. The assay was demonstrated using the Fenton reaction, revealing new insights into the physicochemical aspects of this reaction system with insoluble lignin. In particular, mass solubilized from the film was found to pass through a maximum as a function of the initial concentration of $FeCl_2$ ($[FeCl_2]_o$), with the maximum occurring at $[FeCl_2]_o$ = 1 mM for $[H_2O_2]_o$ = 5%. At that condition, solubilization of mass occurs in two stages. The reaction produces mostly ring-opened products of mass greater than 700 g mol^{-1}, along with a minority of low molecular weight aromatics. The new insight from this work is an important step toward optimizing this complex reaction system for effective lignin breakdown.

Introduction

The valorization of lignin is currently one of the greatest challenges in developing economically viable industries based on lignocellulosic biomass.[1] Lignin is an amorphous polymer that binds cellulose fibrils and hemicellulose into a rigid recalcitrant structure in plant cell walls, and is typically 15–40% of the total dry weight of biomass. While lignin represents the only significant source of renewable aromatics on the planet, currently in the pulp and paper and biofuels industries it is considered a waste stream that is typically burned to generate power and heat. Therefore, lignin represents a significant underutilized source of carbon for conversion to commercial products. Developing cost effective, efficient, and rapid routes to break lignin down into aromatic monomers or other valuable products or precursor chemicals is an intense area of current research.[2–6]

An important bottleneck in converting lignin to valuable products is the efficient breakdown of polymeric lignin into small molecules, suitable for either chemical or biological upgrading.[2–4] The structure and chemistry of lignin varies with the method used for its isolation and separation. Consequently the difficulty of breakdown varies as well. The presence or absence of condensed structures and native ether bonds are factors that most strongly impact the difficulty of further breakdown and conversion. With some lignin breakdown methods, degradation of high molecular weight lignin may be more challenging for water-insoluble forms that arise from most biomass pretreatment processes in biorefineries and from the kraft and organosolv processes in the pulp and paper industry compared to water-soluble forms such as lignosulfonates.

In nature, microbial communities use both enzymatic and catalytic mechanisms to break down lignin. Microbial degradation of lignin has been well studied in fungi (*e.g.*, white rot and brown rot) and in a small number of bacteria, such as

[a]*Joint BioEnergy Institute, Emeryville, CA 94608, USA. E-mail: mskent@sandia.gov*
[b]*Sandia National Laboratories, Livermore, CA and Albuquerque, NM 8718, USA*
[c]*University of California, Berkeley, CA 94720, USA*
†Electronic supplementary information (ESI) available. See DOI: 10.1039/c5gc01083g

Sphingomonas paucimobilis and *Pseudomonas putida*, as reviewed elsewhere.[7–11] White rot fungi are able to mineralize lignin using peroxidases and laccases, very likely in conjunction with small molecule mediators. In comparison, brown rot fungi alter the structure of lignin, but do not mineralize it, using Fenton chemistry.[7,10,12] Some evidence suggests that white rot fungi also utilize Fenton chemistry to some extent in lignin breakdown.[13–20] The breakdown of lignin in nature by bacteria and fungi is typically too slow for industrial applications. Consequently nonnatural catalytic routes to lignin breakdown are under extensive study.[2,6,21]

A major difficulty in the study of lignin breakdown is the lack of a method that is both rapid and highly sensitive for assaying the degradation of polymeric insoluble lignin, since the released fragments are chemically complex and are not easily detected using colorimetric assays. This is in contrast to polysaccharides, in that many methods are available to detect the release of soluble sugars. If the aromatic rings are intact, soluble lignin fragments can be detected through UV absorbance[22,23] or native fluorescence. However the signals are weak and some extent of ring opening often occurs. A common assay for depolymerization of polymeric lignin for many decades has been the mineralization of C14-labeled dehydrogenase polymeric (DHP) lignin to CO_2.[11,24,25] However, DHP lignin is linear and therefore significantly different from the network structure of native lignin. Another approach is to follow changes in the molecular weight distribution of lignin by chromatography.[23,26–28] This approach is difficult to quantify and also has the disadvantage of requiring dissolution of the sample in an organic solvent or aqueous solution of high alkalinity. Since lignin is held together by both covalent and non covalent interactions,[29,30] changing the solvating conditions can substantially alter the structure and will not provide insight into the fragments released in near neutral aqueous processing conditions. Importantly, all the above methods require incubating lignin with enzymes or microorganisms for 7–14 days at a minimum to detect significant changes. In addition, it is challenging to see how these approaches could be used to process a large number of samples in a high throughput or highly multiplexed format.

Two new assays involving polymeric lignin have been reported recently with sufficient sensitivity to detect changes within 20 min upon incubation with culture supernatant of lignolytic bacteria and fungi.[24] One approach involves fluorescently-labeled lignin. In this method, breakdown of lignin results in a change in the environment of the fluorophore (FITC) and therefore a change in the fluorescence spectrum. While sensitive to global changes in lignin structure, the release of soluble fragments is not detected. The second method involves chemically nitrated lignin in which 35–45% of the phenolic rings are nitrated. Release of nitrated low molecular weight phenols results in an increase in UV absorbance at 430 nm. The success of this method in rapidly screening and ranking the lignolytic activity of a set of fungi and bacteria represents a substantial improvement over prior methods. However, the method does not quantify the extent of lignin degradation. Furthermore, while the chemically-altered polymeric lignin is closer in structure to native lignin than low molecular weight compounds or DHP, the chemical structure of the lignin is substantially altered. In particular, as a result of nitration the lignin is soluble in aqueous solution in a manner similar to sulfonation, and therefore is not representative of insoluble native lignin or of the insoluble lignin streams in biorefineries.

Despite this progress, there remains a need for a highly sensitive quantitative assay involving polymeric water-insoluble lignin that can be used in a multiplexed format for rapid, high throughput screening of ligninolytic enzymes, microorganisms, and catalytic chemistries. With intensive efforts underway to discover new enzymes and catalysts, along with the need to optimize reaction conditions, there is a need to conduct large-scale screening and to quantify the extent of lignin breakdown. Regarding optimization of conditions for lignin breakdown, both enzymatic and catalytic approaches are plagued by the tendency for repolymerization of fragments,[30–34] and the physicochemical aspects of this are not fully understood.

We report a new assay based on films of insoluble lignin. In this method, the amount of mass released from the film as soluble fragments is quantified through the decrease in film thickness measured by ellipsometry. The method is quantitative and highly sensitive, as film thickness can be determined to within ±20 Å. While the film format precludes interrogation by NMR, chemical bonding within the film can be studied by surface analytical techniques such as FTIR-ATR or XPS, and the chemical nature of the fragments released can be identified by mass spectrometry, FTIR, and UV-vis. The lignin film assay was developed into a multiplexed format using a silicone mold in the form of a standard 96-well plate. When combined with a lignin film on a standard 4 in silicon wafer, the device enables simultaneous assaying of 76 independent reactions.

The results are presented in two sections. First, studies of stability of the lignin films in various conditions are presented. The assay is then demonstrated by quantifying mass release resulting from the Fenton reaction. The Fenton reaction, in which highly potent hydroxyl radical is generated by reaction of hydrogen peroxide and ferrous salt, is used to treat industrial waste and organic contaminants in groundwater,[35–38] and has been employed in biomass pretreatment strategies.[39–41]

Results

Stability of the lignin films with respect to dissolution in aqueous solutions

In order to study chemical breakdown of lignin deposited as a film, the film must be stable with respect to dissolution under a variety of conditions. This requires adhesion of lignin to the substrate as well as cohesion among the lignin particles within the film. To provide adhesion to the substrate, thin films of polyethyleneimine (PEI) and aminopropyltriethoxysilane (APS) were both examined. Greater adhesion resulted with APS than

with PEI. Care was taken to prepare the adhesion-promoting films without substantially increasing surface roughness or lateral variation in film thickness, as each of these limits the accuracy of the lignin film thickness measurement. Details of film preparation are given in the Methods section. As spun, the lignin films experience gradual release of mass upon incubation against water at pH 4.5 and higher when the liquid is strongly agitated. For example, the film thickness decreases by ~150 Å when individual film pieces are submerged in 2 ml of liquid in a vial and agitated on a shaker at 60 rpm for 4 h. Mass release is most likely due to the solubility of low molecular weight and/or more hydrophilic components within the polydisperse sample. To increase film stability with respect to dissolution in conditions that may arise in lignin breakdown studies such as the presence of agitation, high concentrations of H_2O_2, various buffers, and detergents, the lignin films were exposed to solutions of oxidized 2,2′-azino-bis(3-ethylbenzothiazoline-6-sulfonic acid) (ABTS) as described in the Methods section. Laccase oxidizes ABTS to the stable cation radicals $ABTS^+$ and $ABTS^{2+}$ which oxidize phenolic and non-phenolic structures in lignin, respectively.[42,43] Stability of the ABTS-treated films was first tested by incubation against 1% Tween 20 for 2 h in a shaker at 60 rpm. Film thickness as a function of incubation time against oxidized ABTS and also after subsequent exposure to 1% Tween 20 for 2 h is shown in Fig. 1. Results are shown for films incubated against (i) a solution of 25 μg ml^{-1} laccase and 1 mM ABTS in 10 mM lactate buffer pH 4.5, (ii) a solution of laccase-oxidized ABTS (25 μg ml^{-1} laccase and 1 mM ABTS in 10 mM lactate buffer pH 4.5 incubated for 30 min followed by removal of the laccase by filtration), and (iii) a solution of 1 mM ABTS in the same buffer (no exposure to laccase). For each of these solutions the film thickness initially decreased by ~150 Å and then levelled off after several hours. The fact that the same amount of mass release occurred for unoxidized ABTS as for oxidized ABTS indicates this is likely due to a low level of solubility in the presence of agitation, rather than reaction of oxidized ABTS with the film. However, resistance to the detergent solution (Tween 20) increased markedly with increase in time exposed to oxidized ABTS, and lignin films incubated for 18 h against oxidized ABTS showed no detectable mass release upon incubation with 1% Tween 20 for 2 h. Physical and chemical changes to the lignin upon treatment with oxidized ABTS are described below. Films treated for 18 h with oxidized ABTS are hereafter referred to as base films for the lignin breakdown assays.

Stability of the base lignin films was examined further by incubating small wafer pieces against 2 ml of 10 mM sodium lactate buffer pH 4.5, 1% Tween 20, 1% sodium dodecyl sulfate (SDS), and 1% Triton X-100 for 18 h at room temperature (RT) on a shaker at 60 rpm. No loss of film thickness was detected in the buffer. The results for 18 h incubation in the detergent solutions are shown in Fig. 2. Films treated with oxidized ABTS are highly stable against 1% Tween 20 and 1% SDS, but are only partially stable with respect to 1% Triton X-100. Brief incubation in methanol or dioxane completely removed the films, which shows that the films are not cross-linked but are still composed of independent lignin particles or macromolecules. Upon incubation at 90 °C for 16 h in 50 mM Na malonate buffer pH 4.5 (no agitation) release of ~150 Å was observed. Finally, regarding the effect of pH, the base films are stable for several hours in common buffers at pH 8 without agitation, but substantial mass loss occurs at longer times or upon agitation. Thus, while exposure to oxidized ABTS increases the stability of the films in aqueous solutions, the films are still susceptible to dissolution in organic solvents, or partial dissolution in alkaline solutions, in buffers at high temperatures, or in certain detergent solutions. Nevertheless, such films are entirely suitable for studies involving enzymes or catalytic reactions in aqueous buffers with neutral or acidic pH and near ambient temperature. We note further that the extent of dissolution is a strong function of the agita-

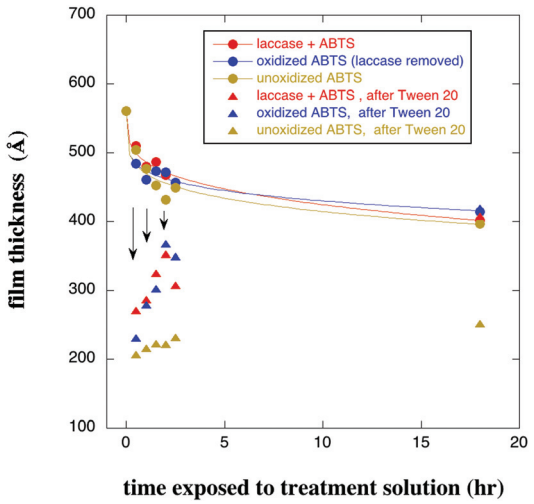

Fig. 1 Film stability in 1% Tween 20 is greatly increased after treatment with oxidized ABTS.

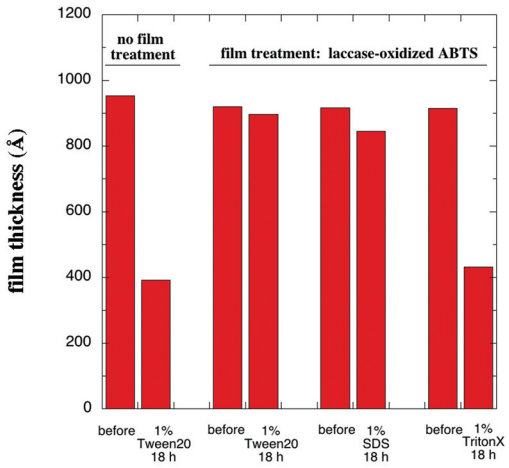

Fig. 2 Film stability in 1% Tween 20 and 1% SDS is greatly increased after treatment with oxidized ABTS.

tion of the liquid. Dissolution is much reduced in 300 μl wells of the multiplexed format to be described below in absence of shaking compared with the level of dissolution that occurs with 2 ml of liquid in a vial on a shaker at 60 rpm.

Characterization of films treated with ABTS

MW distribution. We investigated whether the treatment with laccase-oxidized ABTS alters the molecular weight distribution of the deposited lignin. Crosslinking of lignin by laccase has been reported previously,[44–46] whereas a mixture of laccase and ABTS has been reported to inhibit lignin polymerization.[47] In Fig. 3, a GPC trace of the original lignin material is compared with traces for lignin films recovered from wafers that had (+) or had not (–) been treated with oxidized ABTS. The lignin films were removed from a large number of 3″ diameter silicon wafers using methanol and combined to generate enough material for GPC analysis. The comparison in Fig. 3 shows that treatment with oxidized ABTS does not significantly alter the molecular weight distribution.

Film chemistry. Chemical bonding within the ABTS-treated films was characterized using Fourier transform infrared spectroscopy in attenuated total reflection mode (FTIR-ATR), X-ray photoelectron spectroscopy (XPS), cyclic voltametry, and advancing water contact angles. FTIR spectra were acquired in ATR mode for spin-coated lignin films both before and after treatment with oxidized ABTS. The spectrum for a thick (essentially bulk) film prepared by allowing droplets of 3% lignin in dioxane to evaporate on a Teflon substrate is compared with the spectra of a base lignin film (~900 Å) before and after treatment with oxidized ABTS in Fig. 4. Absorption bands were assigned following prior studies:[48–54] 1706 cm^{-1} C=O stretch in unconjugated ketones, carbonyls, and ester groups with conjugated carbonyls and carboxyls slightly lower toward the 1650 cm^{-1} range; 1598 cm^{-1}, 1514 cm^{-1}, and 1422 cm^{-1} aromatic skeletal vibrations; 1456 cm^{-1} C–H deformation combined with aromatic ring skeletal vibration; 1325 cm^{-1} S ring plus G ring condensed; 1214 cm^{-1} C–O stretch (aryl C–O); 1117 cm^{-1} C–O stretch (ethers) potentially superposed with aromatic C–H in-plane deformation; 1083 cm^{-1} C–H deformation in secondary alcohols and aliphatic ethers; 1031 cm^{-1} aromatic C–H in-plane deformation and C–O stretch (alcohols); and 869 cm^{-1} and 833 cm^{-1} aromatic C–H out of plane deformation. The relation of the band at 1456 cm^{-1} to aromaticity is somewhat ambiguous, since the C–H deformation of CH_3 groups including methoxy occurs in this region as does a strong aromatic ring vibration. The C–O stretch bands are usually observed in the region from 1240–1030 cm^{-1}, and are expected to be in the order of aryl C–O > ether > alcohol and were assigned accordingly. For this region some discrepancy exists in the literature, as a C=O contribution to bands in this region has been suggested.[50,52,54] However, carbonyls are not expected to adsorb in this region.[48] Comparing the spectra for the 900 Å spin-coated film to that of the much thicker film, the absorbance at 1214 cm^{-1} for the thick film has been

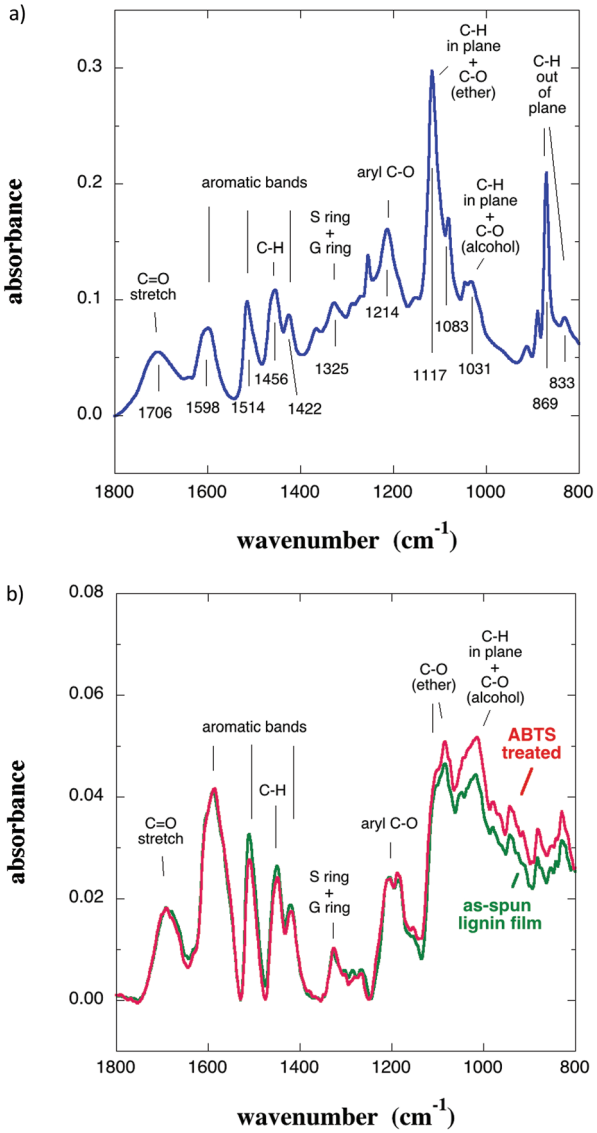

Fig. 4 FTIR spectrum collected in ATR mode for (a) a thick solvent-cast lignin film and (b) a spin-coated 900 Å lignin film before and after treatment with oxidized ABTS.

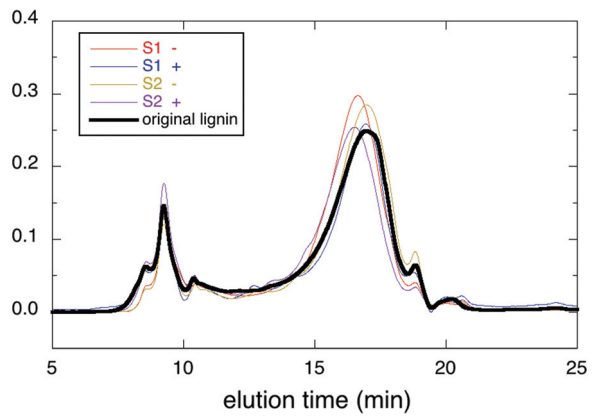

Fig. 3 MW distribution of original lignin material (blue), and lignin recovered from spin-coated films that were (+) or were not (–) treated with oxidized ABTS.

replaced by a doublet at 1200 cm^{-1}. Following others,[48,50,54] we assign these absorbances to C–O stretch of aryl C–O. In addition, the ratio of the bands at 1117 cm^{-1} and 1080 cm^{-1} is altered in the spin-coated 900 Å film such that the band at 1080 cm^{-1} is stronger. The bands for C–H in-plane (1033 cm^{-1}) and out-of-plane (869 cm^{-1} and 833 cm^{-1}) stretches also appear in the spectrum for the spin-coated film with different relative magnitudes compared with the spectrum for the thick film. This could be due to the much weaker signal and effects of background subtraction for the 900 Å film. For the spin-coated lignin film, only very small changes occur upon treatment with oxidized ABTS, indicating that chemical modification of the lignin films upon treatment with oxidized ABTS is relatively weak and not easily detectable by FTIR-ATR.

XPS analysis indicated an increase in oxygen content from 22.3% to 26.1% (O 1s) and a decrease in carbon content from 77.3% to 73.4% (C 1s) upon ABTS treatment. Nitrogen content was less than 0.4% (N 1s).

Cyclic voltammetry was performed on a lignin film after treatment with laccase-oxidized ABTS. A prior study of a lignin film reported a peak corresponding to oxidation of phenolic groups in the initial scan that was replaced by a peak corresponding to oxidation of quinones in subsequent scans.[55] Our results in Fig. 5 show only a reversible quinone redox peak but no phenol peak. This suggests that phenolic groups are oxidized to quinones by the ABTS treatment. Oxidation of phenolic compounds to quinones has been reported previously.[56]

Advancing water contact angles on the base films were time dependent, indicating that surface reconstruction occurred. Values typically decreased from 70° to 63° during a 5 min period. This further shows that the films are not highly cross-linked, but rather contain particles or macromolecules that are able to move independently and rearrange.

In summary, treatment of the lignin films by laccase-oxidized ABTS results in a 3–4% increase in oxygen content, oxidation of phenolic groups to quinones, and no detectable change in the molecular weight distribution.

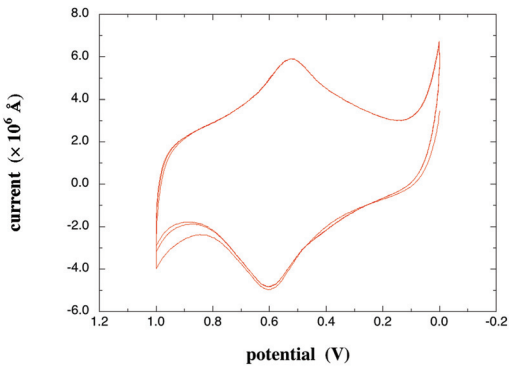

Fig. 5 Cyclic voltamogram of a base lignin film on a gold electrode in 0.5 M sulfuric acid.

Lignin breakdown by the Fenton reaction

The assay was initially performed using individual wafer pieces (~5 mm × 5 mm) with base films and solutions of $[H_2O_2]_o$ = 3% with $[FeCl_2]_o$ of 1 mM and 4 mM at room temperature (RT). The pH was constant throughout the reaction at 3.2 and 2.9 for $[FeCl_2]_o$ of 1 mM and 4 mM, respectively. Results are shown in Fig. 6. Mass release occurred in stages, with a higher rate of mass release within the first 3 hours followed by a lower rate of mass release. The initial rate of mass release was lower for $[FeCl_2]_o$ = 1 mM than for $[FeCl_2]_o$ = 4 mM, but midway through the incubation period the rate of mass release for $[FeCl_2]_o$ = 1 mM increased substantially such that at the end of 18 h substantially greater thickness decrease occurred for $[FeCl_2]_o$ = 1 mM than for $[FeCl_2]_o$ = 4 mM. Incubation in a solution of $[H_2O_2]_o$ = 3% (no $FeCl_2$) resulted in mass release from the films at a much lower level than for the solutions containing $FeCl_2$. Fig. S1 and S2 in the ESI† provide further results for base films incubated in H_2O_2 solutions under different conditions. As discussed further below, mass release in H_2O_2 solutions is most likely due to a slight solubility of the lignin particles at high concentrations of H_2O_2. For the case of $[FeCl_2]_o$ = 4 mM and $[H_2O_2]_o$ = 3% incubated for 18 h, a second treatment resulted in further mass release of comparable magnitude as for the original treatment.

The lignin film assay was subsequently adapted to a multiplexed format using a silicone rubber block containing an array of holes in the pattern of a standard 96-well plate (Fig. S3†). This allows 76 reaction conditions to be assayed simultaneously with a standard 4 in silicon wafer. Fig. 7a shows a photograph of a lignin film-coated silicon wafer following incubation for 18 h against solutions containing

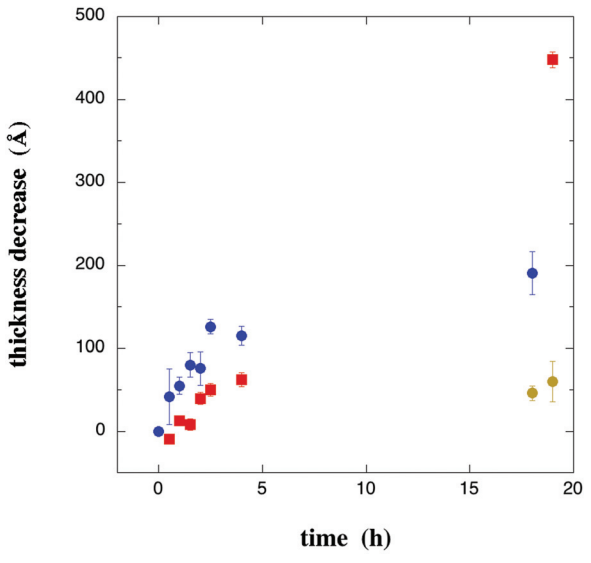

Fig. 6 Decrease in film thickness as a function of time upon exposure of base films to solutions of $[H_2O_2]_o$ = 3% along with $[FeCl_2]_o$ = 4 mM (blue circles), $[FeCl_2]_o$ = 1 mM (red squares), and $[FeCl_2]_o$ = 0 mM (gold circles) at RT.

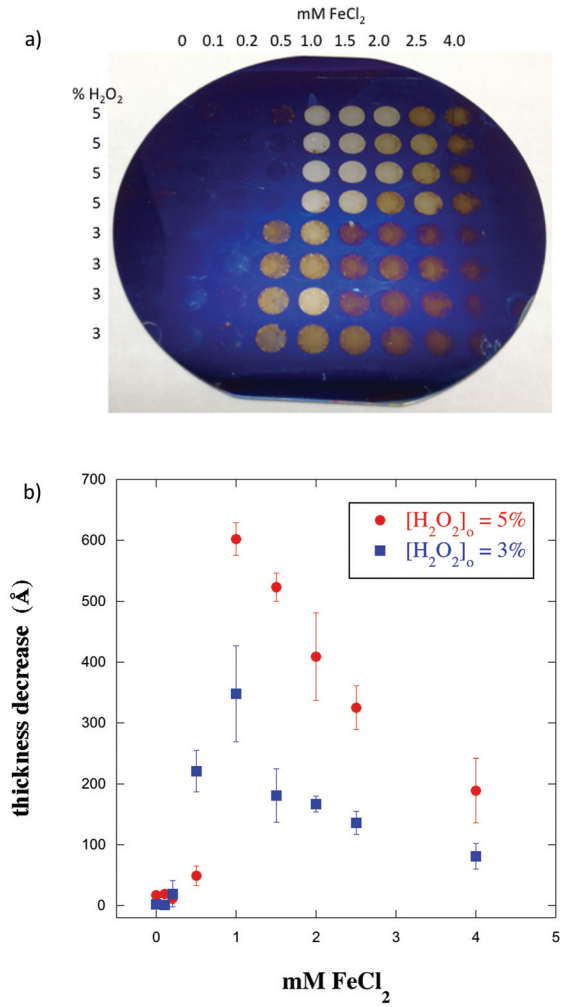

Fig. 7 (a) Photo of a lignin film-coated silicon wafer after use in multiplexed format. The reaction mixtures were incubated against the lignin film for 18 h at RT. (b) Decrease in lignin film thickness as a function of $[FeCl_2]_o$ corresponding to the image in (a).

$[H_2O_2]_o$ of 3% and 5% with $[FeCl_2]_o$ ranging from 0 mM to 4 mM. The pH ranged from 2.96 to 2.83 for $[H_2O_2]_o$ = 3%, and from 2.82 to 2.72 for $[H_2O_2]_o$ = 5%. The decrease in film thickness at the location of each well is plotted in Fig. 7b. Rows 1–4 were identical and rows 4–8 were identical in order to assess reproducibility. The error bars in Fig. 7b are the standard deviation of the four replicates for each condition. The plot shows that mass loss from the film is a nonlinear function of $[FeCl_2]_o$. In particular, there is a sharp increase in mass release over a narrow range of $[FeCl_2]_o$, followed by a slow decline from the maximum with further increase in $[FeCl_2]_o$. Since the initial thickness of the lignin film was about 900 Å, the greatest mass loss corresponds to release of roughly 2/3 of the film. The results also show that only a very low amount of mass is released for $[H_2O_2]_o$ of 3% and 5% in absence of $FeCl_2$. The amount of mass solublized from the film in the presence of $FeCl_2$ increases substantially with $[H_2O_2]_o$. Additional studies indicated that very little mass release occurs for $[H_2O_2]_o \leq 1\%$ over the same range of $[FeCl_2]_o$.

The multiplexed format was also used to study the time dependence of mass release for $[H_2O_2]_o$ = 5% over the same range of $[FeCl_2]_o$ (Fig. 8). Fig. 8a shows that very little mass release occurs for $[FeCl_2]_o$ < 0.5 mM, a large increase in mass release occurs for $[FeCl_2]_o$ between 0.5 mM and 1.0 mM, and mass release after 13 h is substantially greater for $[FeCl_2]_o$ = 1.0 mM than for $[FeCl_2]_o$ = 4.0 mM. Regarding the time course, at $[FeCl_2]_o$ = 1.0 mM there is an initial rapid loss of ~130 Å from the film followed by several hours during which little mass release occurs. Then between 5 h and 10 h mass release occurs at a substantially increased rate. Beyond 10 h the rate of mass release begins to taper off again. For $[FeCl_2]_o$ = 2 mM and $[FeCl_2]_o$ = 4 mM, the shape of the curve is distinctly different from that at $[FeCl_2]_o$ = 1 mM, as shown in Fig. 8b.

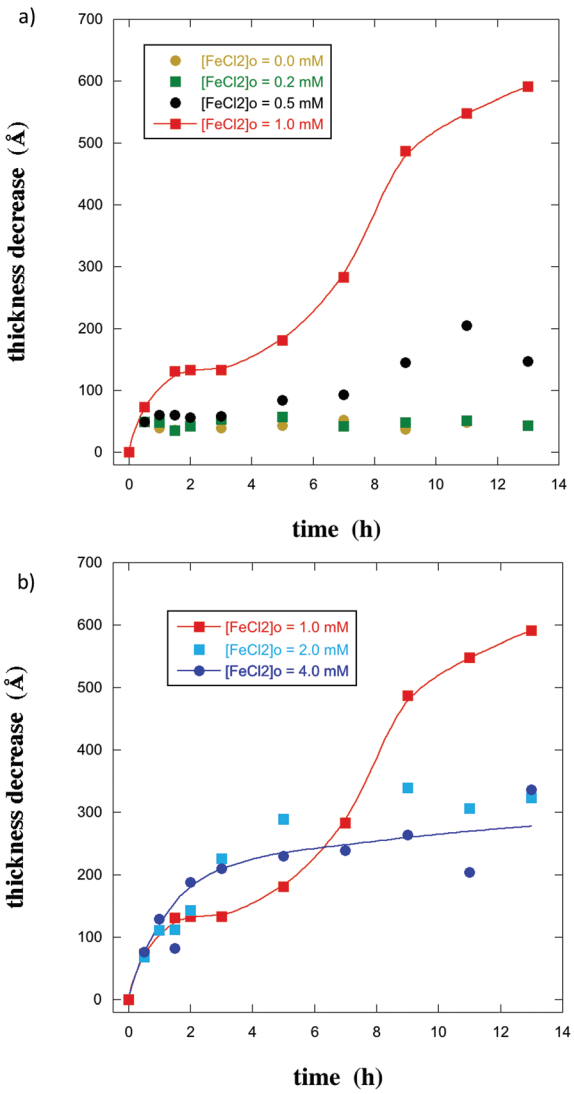

Fig. 8 Decrease in lignin film thickness as a function of time upon incubating against solutions of different $[FeCl_2]_o$ and $[H_2O_2]_o$ = 5% at RT.

Over the first 5 h the mass release is greater for $[FeCl_2]_o$ = 2 mM and $[FeCl_2]_o$ = 4 mM than for $[FeCl_2]_o$ = 1 mM, but the rate of mass release tapers off after that. This is in contrast to the strong increase in the rate of mass release between 5 h and 10 h for $[FeCl_2]_o$ = 1 mM.

FTIR analysis of residual film. FTIR spectra were collected from several locations on the lignin film sample shown in Fig. 7a. The locations scanned correspond to $[FeCl_2]_o$ = 1 mM, 1.5 mM, and 4 mM for $[H_2O_2]_o$ of 3% and 5%. The spectra in the region from 1150 cm^{-1} to 1800 cm^{-1} are compared in Fig. 9. The spectra corresponding to $[FeCl_2]_o$ = 1 mM (reaction conditions giving the maximum mass loss) show substantial changes compared with the spectrum for the original lignin film whereas the spectra for $[FeCl_2]_o$ = 4 mM are similar to that of the original film. While the post-reaction lignin film is substantially thinner for $[FeCl_2]_o$ = 1 mM, the spectra are not simply reduced in magnitude but show distinct changes in the vibrational bands corresponding to chemical differences in the film. In particular, the aromatic bands and the band at 1700 cm^{-1} are greatly diminished and a broad absorbance is observed from 1500 cm^{-1} to 1650 cm^{-1}. These two trends suggest that substantial alteration of the aromatic structures occurred. We propose that opening of aromatic rings leads to conjugated systems of aliphatic C=C and carboxylate (C=O) groups that absorb in the region from 1550 cm^{-1} to 1650 cm^{-1}. Loss of the C=O stretching band at 1700 cm^{-1} is easily explained by a shift to lower wavenumber when acids, aldehydes, and ketones are conjugated with C=C bonds. The spectra corresponding to the intermediate value of $[FeCl_2]_o$ = 1.5 mM are different for the two $[H_2O_2]_o$, correlating with the amount of mass released. For $[H_2O_2]_o$ = 5%, mass released at $[FeCl_2]_o$ = 1.5 mM is 85% of that at $[FeCl_2]_o$ = 1.0 mM and the spectra (Fig. 9b) are very similar for those two conditions. On the other hand, for $[H_2O_2]_o$ = 3% (Fig. 9a), mass released at $[FeCl_2]_o$ = 1.5 mM is only 55% of that at $[FeCl_2]_o$ = 1.0 mM and the spectrum at $[FeCl_2]_o$ = 1.5 mM is intermediate between that at $[FeCl_2]_o$ = 1.0 mM and 4.0 mM, showing a slight decrease in the aromatic peaks and a slight broadening of absorbance from 1500 cm^{-1} to 1650 cm^{-1}.

FTIR spectra obtained for base films before and after 18 h incubation with 3% H_2O_2 (*i.e.* no $FeCl_2$) show no significant changes (Fig. S4†), supporting the conclusion that the low level of mass release in that case is due to solubilization by virtue of H_2O_2 rather than chemical reaction.

UV absorbance of soluble products. UV absorbance spectra of liquids from the wells of the film assay after reaction for $[FeCl_2]_o$ = 1.0 mM and $[FeCl_2]_o$ = 4.0 mM at $[H_2O_2]_o$ = 5% are compared in Fig. 10, along with the spectrum for

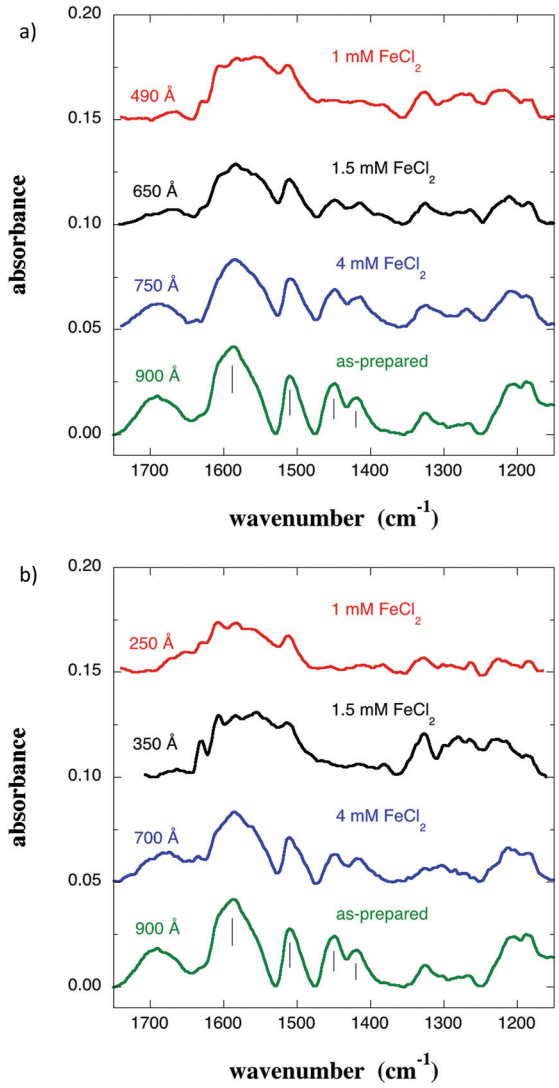

Fig. 9 FTIR spectra from the lignin film shown in Fig. 7a at locations corresponding to various reaction conditions for (a) $[H_2O_2]_o$ = 3%, and (b) $[H_2O_2]_o$ = 5%. Film thicknesses are also indicated.

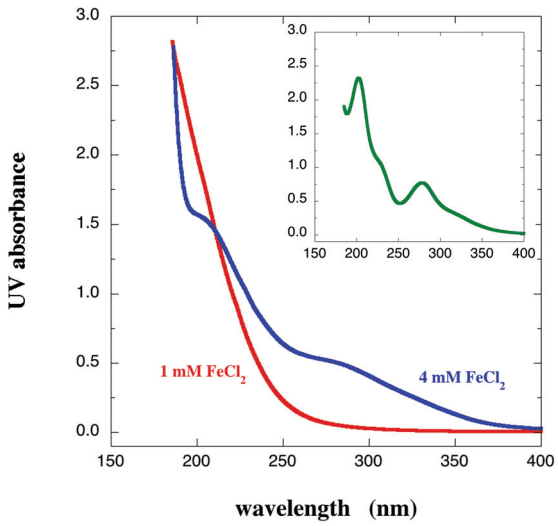

Fig. 10 UV absorbance spectra from reaction liquids for $[FeCl_2]_o$ = 1.0 mM and $[FeCl_2]_o$ = 4.0 mM at $[H_2O_2]_o$ = 5%, indicating substantial chemical differences in the solubilized products. The inset shows the spectrum for the original lignin material (water-soluble fraction).

the water-soluble fraction of the original lignin material. Bands at 205 nm and 280 nm characteristic of lignin are present in the spectrum of the reaction liquid for $[FeCl_2]_o$ = 4.0 mM but are absent in the spectrum for $[FeCl_2]_o$ = 1.0 mM. This indicates that more aromaticity is present in the solubilized products from the reaction involving $[FeCl_2]_o$ = 4.0 mM than for $[FeCl_2]_o$ = 1.0 mM.

FTIR of soluble products. To analyze the soluble products by FTIR-ATR, the liquid from certain wells was removed and evaporated onto Teflon substrates. The material remaining after evaporation was then scraped from the Teflon and pressed against the ATR diamond probe. In Fig. 11a the FTIR absorbance spectrum for the wells corresponding to the last three time points for $[FeCl_2]_o$ = 1 mM in Fig. 8 is compared to the spectrum for the well corresponding to the 11 h time point for $[FeCl_2]_o$ = 4 mM in Fig. 8. These times correspond to the second phase of mass loss, which is strong for $[FeCl_2]_o$ = 1 mM but not observed for $[FeCl_2]_o$ = 4 mM. Upon evaporation the material for $[FeCl_2]_o$ = 4 mM formed a thin film on the Teflon substrate whereas the material for $[FeCl_2]_o$ = 1 mM formed a particle rather than a film. This indicates a substantial difference in the nature of the material for the two conditions. The difference in behavior upon evaporation could be due to a difference in molecular weight distribution or to a difference in the chemical nature of the fragments. The difference is most likely due to a difference in molecular weight, as the IR spectra show the same three major bands in the fingerprint region for $[FeCl_2]_o$ = 1 mM and $[FeCl_2]_o$ = 4 mM. Importantly, the spectra show no evidence for aromatics at either reaction condition. The definitive band for aromatics is 1510–1515 cm^{-1}. The absence of this band for both $[FeCl_2]_o$ = 1 mM and $[FeCl_2]_o$ = 4 mM indicates that aromatics are present in low abundance in both cases, despite the presence of a weak band at 280 nm characteristic of aromatics in the UV spectrum (Fig. 10) for $[FeCl_2]_o$ = 4 mM. We conclude that the soluble material is predominantly comprised of ring-opened products in both cases, but that a small minority of aromatics are present in the solubilized material for $[FeCl_2]_o$ = 4 that are detected in the UV but not in the IR due to the greater sensitivity of UV absorbance to aromatics. While the soluble material is predominantly comprised of ring-opened products in both cases, the distribution of ring-opened products appears to differ somewhat. The absorbance band from 1635 cm^{-1} to 1725 cm^{-1}, corresponding to carbonyl and carboxyl groups, and the band at 1017 cm^{-1} which we assign to the C–O stretch in ethers and alcohols, are much stronger at $[FeCl_2]_o$ = 1 mM than at $[FeCl_2]_o$ = 4 mM relative the broad OH band at 3000–3400 cm^{-1}. We tentatively interpret this as indicating a distribution of products with greater tendency to bind water strongly in the case of $[FeCl_2]_o$ = 4 mM. In addition, the maximum for the broad band at 1530 cm^{-1}–1720 cm^{-1} shifts from 1670 cm^{-1} at $[FeCl_2]_o$ = 1 mM to 1610 cm^{-1} at $[FeCl_2]_o$ = 4 mM. Further work is required to resolve the detailed differences in the distribution of ring-opened products for the two cases.

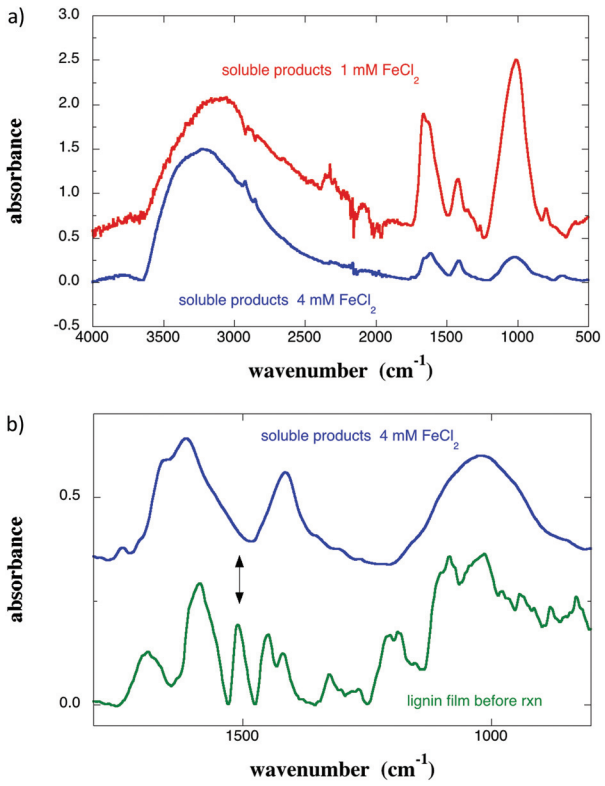

Fig. 11 (a) FTIR spectra from material remaining after evaporation of the liquid from wells corresponding to the last three time points for $[FeCl_2]_o$ = 1 mM in Fig. 8 (red) and from the well corresponding to the 11 h time point for $[FeCl_2]_o$ = 4 mM in Fig. 8 (blue). (b) Expanded view of the spectrum for $[FeCl_2]_o$ = 4 mM in (a) along with the spectrum for the lignin film prior to reaction.

LC-MS analysis of low MW soluble products. Results from LC-MS analyses of soluble products from the Fenton reaction are given in the ESI (Fig. S5–S8†). LC protocols for low MW aliphatic acids, aromatics by atmospheric pressure chemical ionization (APCI), and aromatic acids and aldehydes by electrospray ionization (ESI) were performed. The MS analyses covered molecular weights from 100 g mol^{-1} to 700 g mol^{-1}. Regarding low MW acids, oxalate is present in far greater amounts than either malonate, succinate, or glycolate. Oxalate is present in much greater abundance at $[FeCl_2]_o$ = 4 mM than at $[FeCl_2]_o$ = 1 mM. This is not unexpected as oxalic acid is generated in the oxidation pathway of the other acids, and is the last species generated prior to mineralization.[57] Regarding aromatics by APCI, mass 218.17 is present in far greater amounts than all other masses. This species is present in comparable amounts at $[FeCl_2]_o$ = 1 mM and at $[FeCl_2]_o$ = 4 mM. Regarding aromatic acids and aldehydes by ESI, masses 195.09, 368.27, and 424.33 g mol^{-1} are present in greatest abundance. These species are also present in comparable amounts at $[FeCl_2]_o$ = 1 mM and at $[FeCl_2]_o$ = 4 mM. Importantly, while these data identify the most prominent fragments released in the mass range from 100–700 g mol^{-1}, none of the most abundant species over this mass range is in large excess at $[FeCl_2]_o$ = 1 mM compared with $[FeCl_2]_o$ = 4 mM.

Discussion

The assay described here employs high MW insoluble lignin rather than low MW or soluble forms of lignin as in most other assays of lignin degradation. Moreover, the assay can be performed in aqueous buffers at acidic or near neutral pH, without the need to employ organic solvents or highly alkaline solutions that can alter the physical state of the lignin. The assay is highly sensitive (detects release of as little as 20 Å from the film), potentially enabling detection of ligninolytic activity after short incubation times. While quantitative changes in film thickness from ellipsometric measurements were reported above, changes in film thickness are qualitatively apparent from changes in color. Since the films are ultrasmooth and highly uniform, loss of as little as 30 Å from the films leads to a change in color that is visually observable. This allows for very rapid qualitative assessment of the extent of degradation. An example of the variation of film color with thickness is shown in Fig. 12. Development of the lignin film assay into a multiplexed format allows a large number of reaction conditions to be assayed simultaneously. In this work, organosolv lignin[58] was used as the substrate. However, the assay method is suitable for use with other types of lignin. Organosolv lignin is known to be somewhat recalcitrant to further depolymerization in that it is extensively depolymerized through cleavage of ether bonds during the organosolv process.[59,60] In this work, the lignin films were stabilized against dissolution using laccase-oxidized ABTS. Such films are suitable for use with high concentrations of H_2O_2, neutral or slightly basic conditions, mild agitation, or with lignolytic microbes where rinsing with detergent solutions is required. However, stabilization by treatment with oxidized ABTS is not required for studies of enzymes in buffers at near-neutral or acidic pH in the multiplexed format, as film dissolution is minimal within the 300 μl wells for such conditions in absence of mixing or shaking. Application of this assay at higher temperatures, high pH values, or mixed solvent (aqueous + organic) systems will require more effective methods of stabilizing the lignin particles within the film with respect to dissolution.

Fenton reaction

In general terms, 'Fenton chemistry' can be described as oxidation based on activated hydrogen peroxide, where a redox cycle of Fe(II) and Fe(III) facilitates free radical oxidation with hydrogen peroxide being the primary oxidant. Fe(II) containing oxidizing environments facilitate hydrogen peroxide decomposition to yield hydroxyl and hydroperoxyl radicals as strongly propagating intermediates. Fenton approaches have been used to facilitate degradation of polymers in aqueous and non-aqueous solutions.[61,62] The Fenton reaction system has also been extensively studied for degradation of dilute water-soluble small molecule (mostly aromatic) substrates for water purification. Following Kang *et al.*,[63] the primary reactions in absence of a substrate are given in Table 1. The reactions of this system with certain soluble aromatic compounds are also fairly well understood. For these homogenous reaction conditions, good understanding exists including rate constants for the primary reactions, such that changes in reactant and product concentrations with time have been modelled with reasonable accuracy.[63–68] However, heterogeneous reaction of the Fenton system with insoluble polymeric lignin is much more complex.[69] Lignin fragments generated by reaction with hydroxyl radicals can either recombine with the lignin mass or diffuse away into solution. This is controlled primarily by the solubility of the fragments, but may also be affected by the local density of the lignin (highly condensed or more diffuse). Smaller, more highly oxidized fragments have greater solubility in aqueous solutions and low molecular weight acids are the most commonly observed soluble products when the reactants are present at high concentrations.[40] However, at intermediate oxidation levels, reactions leading to ring opening that generate di-acids can render high MW fragments soluble. Another complicating factor, discussed further below, is that functionalities within partially oxidized lignin can bind Fe(III) and facilitate its reduction to Fe(II).[70]

The reaction pathways of hydroxyl radical with soluble aromatic compounds have been studied in great detail. It was shown previously that hydroxyl radical reacts with aromatic compounds mainly by addition to the ring rather than by reaction with substituents on the ring,[71–75] resulting in hydroxycyclohexadienyl radicals that react further by different pathways depending on reaction conditions such as pH and the presence of O_2, oxidants, or reductants.[64,71,76,77] These different pathways lead to either loss of aromaticity in the

Table 1 Primary reactions of the Fenton system

Reaction	k (M^{-1} s^{-1})
(R1) $Fe^{2+} + H_2O_2 \rightarrow Fe^{3+} + {}^{\bullet}OH + OH^-$	63
(R2) $Fe^{3+} + H_2O_2 \rightarrow Fe^{2+} + H^+ + HO_2^{\bullet}$	0.01
(R3) ${}^{\bullet}OH + H_2O_2 \rightarrow HO_2^{\bullet} + H_2O$	2.7×10^7
(R4) $HO_2^{\bullet} \rightarrow O_2^{-\bullet} + H^+$	1.58×10^5
(R5) $O_2^{-\bullet} + H^+ \rightarrow HO_2^{\bullet}$	1.0×10^{10}
(R6) ${}^{\bullet}OH + Fe^{2+} \rightarrow Fe^{3+} + OH^-$	3.2×10^8
(R7) $HO_2^{\bullet} + Fe^{2+} (+H^+) \rightarrow Fe^{3+} + H_2O_2$	1.2×10^6
(R8) $HO_2^{\bullet} + Fe^{3+} \rightarrow Fe^{2+} + H^+ + O_2$	3.1×10^5
(R9) $O_2^{-\bullet} + Fe^{2+} (+2H^+) \rightarrow Fe^{3+} + H_2O_2$	1.0×10^7
(R10) $O_2^{-\bullet} + Fe^{3+} \rightarrow Fe^{2+} + O_2$	5×10^7
(R11) ${}^{\bullet}OH + {}^{\bullet}OH \rightarrow H_2O_2$	4.2×10^9
(R12) $HO_2^{\bullet} + HO_2^{\bullet} \rightarrow H_2O_2 + O_2$	8.3×10^5
(R13) ${}^{\bullet}OH + HO_2^{\bullet} \rightarrow O_2 + H_2O$	1×10^{10}
(R14) ${}^{\bullet}OH + O_2^{-\bullet} \rightarrow O_2 + OH^-$	1×10^{10}
(R15) $HO_2^{\bullet} + O_2^{-\bullet} (+H^+) \rightarrow H_2O_2 + O_2$	9.7×10^7

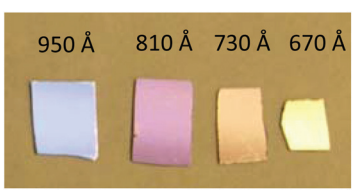

Fig. 12 Variation in film color with thickness.

form of cyclohexadienyl species or ring-opened products, or various products in which the aromatic rings are retained. The latter includes condensation reactions of two rings and also formation of various phenols. For interaction of hydroxyl radicals with lignin, the same reaction pathways have been reported, along with displacement of methoxy groups and cleavage of β-O-4 ether bonds.[14,70,78,79]

Understanding the factors that control these reaction pathways in the context of the heterogeneous reaction with insoluble lignin will result in the potential for reaction optimization, including control over the product distribution and the yield of soluble products, and more efficient use of the expensive reagent H_2O_2.

The data in Fig. 6–8 for the heterogeneous reaction of the Fenton system with lignin films show several features that contrast with the results of prior studies involving homogenous reactions with dilute soluble aromatic substrates. First, much higher $[H_2O_2]_o$ is needed to achieve significant mass release from lignin films compared with that required to degrade dilute soluble substrates. Specifically, Fig. 7 shows that mass release from the lignin films during an 18 h incubation is substantially lower for $[H_2O_2]_o$ = 3% compared with $[H_2O_2]_o$ = 5%, and further studies (not shown) indicate that very little mass release is observed for $[H_2O_2]_o \leq 1\%$ (= 294 mM). In contrast, $[H_2O_2]_o$ = 10–20 mM is adequate to degrade dilute soluble substrates for $[FeCl_2]_o$ in the mM range.[63–68] Second, at $[FeCl_2]_o$ = 1 mM mass release occurs in two stages (Fig. 8). In contrast, the degradation of dilute soluble aromatic substrates typically occurs within a few tens of minutes at mM concentrations of $FeCl_2$ and H_2O_2 and there appears to be only a single stage in the reaction.[63–65] Third, the amount of mass solubilized from the lignin film during an 18 h incubation goes through a maximum as a function of $[FeCl_2]_o$ whereas the rate of degradation of soluble aromatic substrates increases monotonically with $[FeCl_2]_o$.[63–65] Each of these aspects will be discussed further below.

Prior to discussing possible mechanisms to account for these observations, we first summarize the analytical results for the soluble products. The IR data for the soluble products indicate that the main components are carboxylic acids, aldehydes, ketones, ethers, and alcohols, and the lack of detectable aromatic bands indicates that aromatics are present in small amounts for both $[FeCl_2]_o$ = 1 mM and $[FeCl_2]_o$ = 4 mM. With UV absorbance, which is more sensitive to aromatics than IR, aromatics were detected at $[FeCl_2]_o$ = 4 mM but not at $[FeCl_2]_o$ = 1 mM. LC-MS has the greatest sensitivity of the three methods, but only covered the mass range from 100–700 g mol^{-1}. Aromatics were detected at $[FeCl_2]_o$ = 1 mM and at $[FeCl_2]_o$ = 4 mM, and the most prominent species were at roughly the same abundance in the two cases. From this it follows that the aromatic signal detected by UV absorbance for $[FeCl_2]_o$ = 4 mM but absent for $[FeCl_2]_o$ = 1 mM must arise from molecular weights greater than 700 g mol^{-1}. Furthermore, the fact that no species was present in substantially greater abundance at $[FeCl_2]_o$ = 1 mM than at $[FeCl_2]_o$ = 4 mM in the MS spectrum indicates that the solublized species corresponding to the greater mass loss at $[FeCl_2]_o$ = 1 mM (four fold excess at $[H_2O_2]_o$ = 5% relative to that at $[FeCl_2]_o$ = 4 mM) must also have molecular weights greater than 700 g mol^{-1}.

Regarding the physicochemical mechanisms of the Fenton system with insoluble lignin, the requirement for higher $[H_2O_2]_o$ for mass release from insoluble lignin films may simply reflect the fact that multiple oxidation reactions are needed to generate fragments that are sufficiently soluble to diffuse into solution rather than remain with the lignin film. This is especially true for solubilization of higher MW fragments. Another possible explanation is enhanced coupling between hydroxycyclohexadienyl radicals. Prior studies of the reaction of hydroxyl radical with dilute soluble (low MW) aromatics have shown that coupling of two hydroxycyclohexadienyl radicals is favored in the absence of O_2 or oxidants.[64,73,77] Coupling of two hydroxycyclohexadienyl radicals is likely to be more strongly favored when localized within insoluble lignin particles compared to freely diffusing soluble substrates. Such coupling reactions would not result in the release of mass from the film. For the heterogeneous Fenton reaction with a film of insoluble lignin particles, a much higher concentration of oxidant may be required to bias the reaction away from such coupling reactions. Third, a higher $[H_2O_2]_o$ may provide a more solubilizing environment for fragments generated from the reaction.

Mass release from the film passes through a maximum because the second stage of mass release is much stronger at $[FeCl_2]_o$ = 1 mM than at $[FeCl_2]_o$ = 4 mM. We emphasize the remarkable finding that greater mass release from the film occurs at lower oxidizing power over this range. Regarding the two stages of mass release we propose that the first stage is due to hydroxyl radical generated by reaction of the initial concentration of Fe(II) with H_2O_2 as in eq. R1 (Table 1). We propose that the second stage of mass loss occurs upon gradual reduction of Fe(III) to Fe(II), thereby generating additional hydroxyl radical. This is supported by the fact that the second phase of mass loss occurs at reaction times between 5 and 10 hours, which are much longer than required for complete reaction of the initial concentration of Fe(II).[63–66] Reduction of Fe(III) to Fe(II) is likely to result from the interaction of Fe(III) with dihydroxy aromatics or acids within the lignin.[70] A number of studies have shown that various *ortho* dihydroxy aromatic compounds and acids are able to reduce Fe(III) to Fe(II).[17,80–82] The interaction of hydroxyl radical with lignin is known to result in replacement of methoxy groups with hydroxyls, which would leave an abundance of *ortho* dihydroxyl aromatic moieties.[14] We propose that either acid or dihydroxy aromatic functionalities bind and reduce Fe(III) to Fe(II) producing the second stage of mass release for $[FeCl_2]_o$ = 1 mM.

In addition to explaining the origin of the second stage of mass release, this mechanism also explains why the second state is much more efficient at solublizing mass from the film than the first stage. During the first stage the amount of mass solubilized is greater at $[FeCl_2]_o$ = 4 mM than at $[FeCl_2]_o$ =

1 mM, as expected based on the higher concentration of hydroxyl radical. However, the second stage is much more efficient at releasing mass from the film, resulting in greater total mass release at $[FeCl_2]_o$ = 1 mM than at $[FeCl_2]_o$ = 4 mM. If, as postulated here, the second stage is due to Fe(III) chelation and reduction by dihydroxy aromatic moieties within the lignin, then hydroxyl radicals will be generated in close proximity to the aromatic rings. We postulate that this leads to ring opening and generation of carboxylic acid groups that solubilize high molecular weight fragments in a manner that is very efficient with respect to usage of hydroxyl radicals. This is supported by the FTIR (residual films) and UV absorbance data showing that greater ring opening occurs at $[FeCl_2]_o$ = 1 mM than at $[FeCl_2]_o$ = 4 mM.

If, as hypothesized here, the second stage of degradation is due to reduction of Fe(III) to Fe(II), then it follows that at $[FeCl_2]_o$ = 4 mM the reduction of Fe(III) to Fe(II) is suppressed. One possibility is that reduction of Fe(III) to Fe(II) is suppressed at $[FeCl_2]_o$ = 4 mM due to much higher oxalic acid concentration generated in that case (ESI, Fig. S5†). Decreased capacity of organic compounds to reduce Fe(III) to Fe(II) is known to occur with increasing oxalic acid concentration due to the formation of highly stable Fe-oxalate complexes.[83] In particular, prior work has shown that excess oxalic acid inhibits Fe(III) reduction by dihydroxy aromatic compounds.[17,81] Further work is needed to confirm this hypothesis in the present case.

Alternatively, the possibility of different degradation pathways at $[FeCl_2]_o$ = 1 mM and $[FeCl_2]_o$ = 4 mM is suggested by prior work showing that the decay of hydroxycyclohexadienyl radicals to yield ring fragmentation products becomes more significant with increasing concentration of O_2, whereas the formation of phenols is favored in the presence of a strong oxidant.[64,71,77] The UV data showing detectable aromatics at $[FeCl_2]_o$ = 4 mM but no detectable aromatics at $[FeCl_2]_o$ = 1 mM is consistent with the possibility that different decay pathways may be involved. However, the IR data in Fig. 11 show that in both cases the majority of solubilized products are ring-opened species. The fact that the majority of solubilized products are the same in the two cases indicates that any difference in chemical degradation pathways is a minor effect. We suggest that the greater amount of ring opening and mass release at $[FeCl_2]_o$ = 1 mM is most likely the result of oxidation of rings of aromatic moieties that chelated and reduced Fe(III) to Fe(II) during the second phase.

Conclusion

With a high sensitivity and multiplexed format, this new assay should be useful for rapid assessment of catalytic, enzymatic, and microbial degradation of insoluble lignin. Furthermore, it can provide new fundamental insights into physicochemical processes involved in lignin degradation, as demonstrated here in the discovery of the nonlinear dependence of mass solubilization on $[FeCl_2]_o$ for the Fenton reaction system. Time course studies showed that the increased solubilization of mass at $[FeCl_2]_o$ = 1 mM corresponds to a second phase that is not present at $[FeCl_2]_o$ = 4 mM. We attribute this second phase of mass release to the gradual reduction of Fe(III) to Fe(II) by dihydroxy aromatic moiesties or aromatic acids generated within the lignin. We suggest that reduction of Fe(III) to Fe(II) is suppressed at $[FeCl_2]_o$ = 4 mM due to generation of a higher concentration of oxalic acid in that case. However, other possible interpretations may exist and further work is needed to definitely resolve the mechanisms leading to the nonlinear behavior with $[FeCl_2]_o$. The reaction produces mostly ring-opened products along with a small minority of aromatics. The yield of aromatics is lower at $[FeCl_2]_o$ = 1 mM than at $[FeCl_2]_o$ = 4 mM. Taken together the data suggest that the majority of solubilized fragments have molecular weights greater than 700 g mol^{-1}. This work shows that a thorough understanding of this complex heterogeneous reaction system is necessary in order to optimize it for transforming lignin into more useful products or intermediates.

Experimental

Materials

Organosolv lignin was obtained from Lignol Corp. This material has a bimodal molecular weight distribution. The larger peak of the two peaks is the lower molecular weight fraction, which has M_n = 4250 g mol^{-1}, M_w = 9700 g mol^{-1} by GPC based on calibration with polystyrene standards. Aminopropyltriethoxysilane (APS), polyethyleneimine (PEI, MW = 60 000 g mol^{-1}), $FeCl_2$, Triton X-100, and 2,2′-azino-bis(3-ethylbenzothiazoline-6-sulfonic acid) diammonium salt were purchased from Sigma-Aldrich. H_2O_2 (~35%) and sodium dodecyl sulfate were purchased from Fisher Scientific. Tween 20 was purchased from Fisher Biotech. Laccase from *T. versicolor* (10 U mg^{-1}) was purchased from US Biological. Silicon wafers were undoped type N with 1–0–0 orientation.

Methods

Preparation of lignin films. Prior to coating the silicon substrates with liginin, films of either PEI or APS were deposited to promote adhesion. Silicon wafers (4 in diameter) were first cleaned with detergent solution followed by UV-ozone treatment for 30 min. PEI was deposited by dip coating following a prior report.[84] The wafers were placed into a 0.5% solution of PEI in water for 10 min, then removed and rinsed with water, and dried with nitrogen. Smooth films of APS were deposited onto UV-ozone cleaned silicon wafers by spin coating. APS was dissolved into 90/10 ethanol/water at 0.25% and stirred for 60 min. The solution was then spin coated onto the silicon wafers at 3000 rpm. The APS-coated wafers were then heated in vacuum at 70 °C for 1 h to drive off the water and cure the film.

Lignin was dissolved at 2% or 3% in 1,4-dioxane, filtered through a 1 μM syringe filter, and spin coated onto silicon wafers using a Headway photo resist spinner model

1-PM101DT-R790.[34,85] A range of spinning speeds (2000–4000 rpm) and accelerations (2–9) were explored to maximize film uniformity. The lignin-coated wafers were then heated in vacuum at 70 °C for 1 h to drive off the dioxane. At 4000 rpm and acceleration of 9.0, film thicknesses were 560 ± 20 Å and 950 ± 20 Å for 2% and 3%, respectively. Adhesion of the lignin film to the substrate was tested by (i) 18 h treatment with 1 mM laccase-oxidized ABTS, and (ii) submerging the films resulting from (i) in 3% H_2O_2 at 60 °C for 1 h.

Treatment of films with oxidized ABTS. Laccase (25 μg ml^{-1}) was added to a 1 mM solution of ABTS in 10 mM sodium lactate buffer pH 4.5 and allowed to catalyze the oxidation of ABTS for 30 min. UV absorbance indicated that under these conditions the maximum concentration of oxidized ABTS is achieved after incubation for 20 min (Fig. S9†). Following incubation for 30 min, the solution was filtered through a 10 000 g mol^{-1} molecular weight cutoff (MWCO) filter to remove the laccase. The lignin films were then incubated against the solution of oxidized ABTS. Following the desired incubation times, the samples were removed and then rinsed thoroughly with Millipore water.

For some assays, the ABTS-treated lignin-coated wafers were cut into samples roughly 5 mm × 5 mm by scribing the back of the wafer.

Film thickness measurements. Film thickness measurements involving individual lignin-coated wafer samples were performed using a Nanofilm EP3 ellipsometer (Accurion GmbH). A minimum of three measurements (at 70° and 532 nm) per sample were collected and averaged. For the multiplexed format, film thickness measurements were automated using a NanoSpec 6100 spectral reflectometer from Nanometrics, with a wavelength range of 480–800 nm. By means of a motorized sample stage and a pre-defined test pattern, the tool semi-autonomously measured each well location (*i.e.*, once the location of the first test site was verified, no further intervention was required). Pre-reaction data were collected with one measurement per well location. Post-reaction data were collected in triplicate—once with the measurement site in the center of the well, again with the site offset slightly above the center line, and a third offset slightly below the centerline.

Gel permeation chromatography (GPC). GPC was performed with as-received lignin and also with lignin recovered from films, either untreated or treated with oxidized ABTS. An Agilent 1200 series binary LC system (G1312B) equipped with DA (G1315D) detector was used. Separation was achieved with a Shodex SB-803 column (6 μm particle size, 300 mm × 8.0 mm i.d., Showa Denko America, Inc., New York, NY, USA) at 80 °C using a mixture of *N*-methyl-2-pyrrolidinone and dimethyl sulfoxide (1 : 1 (v/v)) as the mobile phase at a flow rate of 0.5 ml min^{-1}. Absorbance of materials eluting from the column was detected at 290 nm. Intensities were area normalized.

LC-MS. Aromatic alcohols were analyzed by HPLC—atmospheric pressure chemical ionization (APCI)—time-of-flight mass spectrometry (TOF MS). Separation of these compounds was conducted on an Agilent 1200 Series Rapid Resolution HPLC system (Agilent Technologies Inc., Santa Clara, CA, USA) using an Eclipse Plus Phenyl-hexyl column (250 mm length, 4.6 mm inside diameter, and 5 μm particle size; Agilent Technologies, Santa Clara, CA). The mobile phase was composed of 0.1% formic acid in water (solvent A) and methanol (solvent B). The elution gradient was as follows: from 30% B to 98% B in 20 min, held at 98% B for 5 min, reduced from 98% B to 30% B in 0.5 min, and held at 30% B for a further 3 min. A flow rate of 0.5 mL min^{-1} was used until 25 min, after which it was increase to 1 mL min^{-1} in 0.5 min and held at this flow rate for an additional 3 min. The total run time was 28.5 min. The column compartment and sample tray were set to 50 °C and 4 °C, respectively. The HPLC system was coupled to an Agilent Technologies 6210 LC/TOF mass spectrometer with a 1 : 5 post-column split. Mass spectrometric detection was conducted using APCI in the positive ion mode. MS experiments were carried out in the full scan mode, at 0.86 spectra per second, for the detection of $[M–H_2O + H]^+$ or $[M + H]^+$ ions. Drying and nebulizing gases were set to 11 L min^{-1} and 30 lb per in^2, respectively, and a drying gas temperature of 330 °C was used throughout. The vaporizer and corona were set to 350 °C and 4 μA respectively, and a capillary voltage of 3500 V was also used. Fragmentor and OCT 1 RF voltages were each set to 170 V, while the skimmer voltage was set to 50 V. Data acquisition and processing were performed by the MassHunter software package (Agilent Technologies).

Aromatic acids and aldehydes were analyzed by HPLC and electrospray ionization (ESI) TOF MS using a method modified from that described previously,[86] with further detail as follows. Separation of these compounds was conducted *via* the aforementioned column and HPLC system. A sample injection volume of 5 μl was used throughout. The sample tray and column compartment were set to 4 and 50 °C, respectively. The mobile phase was composed of 10 mM ammonium acetate (Sigma-Aldrich) in water (solvent A) and 10 mM ammonium acetate in 90% acetonitrile and 10% water (solvent B). The mobile phases were made up from a stock solution of 100 mM ammonium acetate and 0.7% formic acid (Sigma-Aldrich) in water. The elution gradient was as follows: from 30% B to 98% B in 20 min, held at 98% B for 5 min, reduced from 98% B to 30% B in 0.5 min, and held at 30% B for a further 3 min. A flow rate of 0.5 mL min^{-1} was used until 25 min, after which it was increase to 1 mL min^{-1} in 0.5 min and held at this flow rate for an additional 3 min. The total run time was 28.5 min. The HPLC system was coupled to an Agilent Technologies 6210 series time-of-flight mass spectrometer (for LC-TOF MS) *via* a MassHunter workstation (Agilent Technologies, CA). Drying and nebulizing gases were set to 11 L min^{-1} and 30 lb per in^2, respectively, and a drying-gas temperature of 330 °C was used throughout. ESI was conducted in the negative ion mode and a capillary voltage of −3500 V was utilized. MS experiments were carried out in the full scan mode, at 0.86 spectra per second, for the detection of $[M - H]^-$ ions. Data acquisition and processing were performed by the MassHunter software package (Agilent Technologies).

Organic acids were analyzed as previously described by Juminaga *et al.*[87]

UV. UV absorbance spectra were collected on reaction liquids using a JASCO J815 spectrometer. Samples were diluted in Millipore water as necessary.

FTIR. FTIR spectra were collected from lignin-coated wafers using a Bruker Hyperion IR Microscope equipped with a single-bounce germanium attenuated total reflectance (ATR) objective. A total of 512 scans were co-added. Spectral resolution was 4 cm^{-1}. Spectra were referenced to air and an atmospheric correction applied to the data to remove water and CO_2 vapor contributions. An average of 5 spectra collected from each sample location was used for further analysis and interpretation. Spectra were baseline corrected by fitting a second order polynomial to the spectral region 800–1800 cm^{-1}.

FTIR spectra were also collected from residual solid material after evaporating reaction liquids onto Teflon substrates. The material was scraped from the Teflon substrate and pressed against a Pike GladiATR diamond ATR single reflection crystal. IR spectra were collected with a Bruker Equinox 55 IR spectrometer with a DTGS (ID301/8) detector operating at room temperature. A total of 32 scans were co-added. Spectral resolution was 4 cm^{-1}. Spectra were referenced to air and an atmospheric correction applied to the data to remove water and CO_2 vapor contributions. Spectra were baseline corrected by fitting a second order polynomial to the spectral region.

XPS. XPS was performed using a Kratos Axis Ultra DLD instrument with a monochromatic Al Kα (1486.7 eV) X-ray source operated at 150 W. The analysis area was an elliptical spot of 300 × 700 microns and samples were analyzed at a 90° take-off angle with respect to the analyzer. Base pressures for the instrument were less than 5×10^{-9} Torr. Survey spectra were taken with an 80 eV pass energy, 500 meV step, and 100 ms dwell times. High resolution spectra were recorded with a 20 eV pass energy, 100 ms dwell time, and step sizes ranging from 50–100 meV. Data processing was performed with CasaXPS Version 2.3.15.

Cyclic voltammetry. Cyclic voltammetric scans were run using a VoltaLab PGZ402 (Radiometer analytical) in 0.5 M H_2SO_4 at 100 mV s^{-1} *versus* an Ag/AgCl and Pt reference and counter electrode respectively.

Water contact angles. Advancing water contact angle measurements were made with a Kruss DSA10-MK2 drop shape analyzer using Millipore water (18.2 MΩ). Reported values are averages of three measurements.

Multiplexed format. A multiplexed format was developed by fabricating a silicone rubber block containing an array of holes in the pattern of a standard 96-well plate. This was achieved by first fabricating a negative mold from a standard 96-well bottomless plastic plate, and then using the mold to fabricate the silicone block with the array of holes. The device (shown in Fig. S3†) is comprised of an aluminum base plate, a standard 4 in silicon wafer, the silicone block with the array of holes in the pattern of a 96-well plate, the plastic bottomless 96-well plate used to create the mold, and then finally an aluminum top plate with a window cut out to allow access to the wells. Including the plastic bottomless 96-well plate between the silicone part and the aluminum top plate helped to apply a uniform pressure on the silicone form around each hole and prevent leakage between the wells.

For measurements in the multiplexed format, initial thickness measurements were made for a 4 in wafer with lignin film at the locations corresponding to the reaction wells. The device was then assembled, tested for leaks with Millipore water, and then the solutions of $FeCl_2$ and H_2O_2 were pipetted into each well (300 µl per well). Millipore water adjusted to pH 3 with HCl was used to prepare the solutions. The reactions were initiated by addition of H_2O_2. An adhesive film was then placed over the top of the wells to minimize evaporation during the reaction. After the desired incubation period, the liquid was removed from each well and frozen until analysis by LC-MS, FTIR, or UV. Immediately after removing the liquid from each well, the well was rinsed three times with 300 µl aliquots of Millipore water to avoid further reaction. The device was then disassembled and the entire wafer rinsed with Millipore water and dried with a stream of nitrogen. For time course measurements, after the liquid from a well was removed at the intended time the well was rinsed two times with 300 µl of Millipore water and then another 300 µl aliquot of pure Millipore water was left in the well until the completion of the trial. Final thickness measurements were then made using the same grid pattern.

Acknowledgements

This work conducted by the Joint BioEnergy Institute (http://www.jbei.org) was supported by the Office of Science, Office of Biological and Environmental Research, of the U.S. Department of Energy under Contract No. DE-AC02-05CH1123. This work was also supported by the Laboratory Directed Research and Development program at Sandia National Laboratories. Sandia National Laboratories is a multi-program laboratory managed and operated by Sandia Corporation, a wholly owned subsidiary of Lockheed Martin Corporation, for the U.S. Department of Energy's National Nuclear Security Administration under contract DE-AC04-94AL85000. Part of this work was performed at the Center for Integrated Nanotechnologies, a US Department of Energy, Office of Basic Energy Sciences user facility at Low Alamos National Laboratory (contract DE-AC52-06NA25396) and Sandia National Laboratories.

References

1 B. A. Simmons, D. Loque and J. Ralph, Advances in modifying lignin for enhanced biofuel production, *Curr. Opin. Plant Biol.*, 2010, **13**, 313–320.

2 J. Zakzeski, *et al.*, The catalytic valorization of lignin for the production of renewable chemicals, *Chem. Rev.*, 2010, **110**, 3552–3599.
3 M. P. Pandey and C. S. Kim, Lignin depolymerization and conversion: A review of thermochemical methods, *Int. J. Biochem. Mol. Biol.*, 2011, **34**, 29–41.
4 A. J. Ragauskas, *et al.*, Lignin valorization: improving lignin processing in the biorefinery, *Science*, 2014, **344**, 1246843.
5 J. G. Linger, *et al.*, Lignin valorization through integrated biological funneling and chemical catalysis, *Proc. Natl. Acad. Sci. U. S. A.*, 2014, **111**, 12013–12018.
6 A. Rahimi, *et al.*, Formic-acid-induced depolymerization of oxidized lignin to aromatics, *Nature*, 2014, **515**, 249–252.
7 T. D. H. Bugg, *et al.*, Pathways for degradation of lignin in bacteria and fungi, *Nat. Prod. Rep.*, 2011, **28**, 1883–1896.
8 K. E. Hammel and D. Cullen, Role of fungal peroxidases in biological ligninolysis, *Curr. Opin. Plant Biol.*, 2008, **11**, 349–355.
9 F. J. Ruiz-Duenas and A. T. Martinez, Microbial degradation of lignin: how a bulky recalcitrant polymer is efficiently recycled in nature and how we can take advantage of it, *Microb. Biotechnol.*, 2009, **2**, 164–177.
10 A. Hatakka, Biodegradation of lignin, in *Biopolymers. Lignin, Humic Substrances, and Coal. A multivolume handbook*, ed. A. Steinbuchel and M. Hofrichter, Wiley-VCH, Weinheim, Germany, 2001.
11 W. Zimmerman, Degradation of lignin by bacteria, *J. Biotechnol.*, 1990, **13**, 119–130.
12 V. Arantes, J. Jellison and B. Goodell, Peculiarities of brown-rot fungi and biochemical Fenton reaction with regard to their potential as a model for bioprocessing biomass, *Appl. Microbiol. Biotechnol.*, 2012, **94**, 323–338.
13 B. Bes, R. Ranjev and A. M. Boudet, Evidence for the involvement of activated oxygen in fungal degradation of lignocellulose, *Biochimie*, 1983, **65**, 283–289.
14 K. E. Hammel, *et al.*, Reactive oxygen species as agents of wood decay by fungi, *Enzyme Microb. Technol.*, 2002, **30**, 445–453.
15 P. Kersten and D. Cullen, Extracellular oxidative systems of the lignin-degrading Basidiomycete Phanerochaete chrysosporium, *Fungal Genet. Biol.*, 2007, **44**, 77–87.
16 V. Gomez-Toribio, *et al.*, Induction of extracellular hydroxyl radical production by white rot fungi through quinone redox cycling, *Appl. Environ. Microbiol.*, 2009, **75**, 3944–3953.
17 V. Arantes, *et al.*, Lignocellulosic polysaccharides and lignin degradation by wood decay fungi: the relevance of nonenzymatic Fenton-based reactions, *J. Ind. Microbiol. Biotechnol.*, 2011, **38**, 541–555.
18 S. Backa, *et al.*, Hydroxyl radical activity associated with the growth of white-rot fungi, *Holzforschung*, 1993, **47**, 181–187.
19 S. M. Kremer and P. M. Wood, Production of Fenton's reagent by cellobiose oxidase from cellulolytic cultures of Phanerochaete chrysosporium, *Eur. J. Biochem.*, 1992, **208**, 807–814.
20 H. Tanaka, S. Itakura and A. Enoki, Hydroxyl radical generation by an extracellular low-molecular-weight substance and phenol oxidase activity during wood degradation by the white-rot basidiomycete Trametes versicolor, *J. Biotechnol.*, 1999, **75**, 57–70.
21 T. Parsell, *et al.*, A synergistic biorefinery based on catalytic conversion of lignin prior to cellulose starting from lignocellulosic biomass, *Green Chem.*, 2015, **17**, 1492–1499.
22 J. Jansekar, C. Brown and A. Fiechter, Determination of biodegraded lignin by ultraviolet spectrophotometry, *Anal. Chim. Acta*, 1981, **130**, 81–91.
23 D. C. Ulmer, *et al.*, Rapid degradation of isolated lignins by Phanerochaete chrysosporium, *Appl. Environ. Microbiol.*, 1983, **45**, 1795–1801.
24 M. Ahmad, *et al.*, Development of novel assays for lignin degradation: comparative analysis of bacterial and fungal lignin degraders, *Mol. BioSyst.*, 2010, **6**, 815–821.
25 T. K. Kirk, *et al.*, Preparation and microbial decomposition of synthetic [14C]-lignins, *Proc. Natl. Acad. Sci. U. S. A.*, 1975, **72**, 2515–2519.
26 K. E. Hammel, *et al.*, Ligninolysis by a purified lignin peroxidase, *J. Biol. Chem.*, 1993, **268**, 12274–12281.
27 M. G. S. Chua, S. Choi and T. K. Kirk, Mycelium binding and depolymerization of synthetic 14C-labeled lignin during decomposition by Phanerochaete chrysosporium, *Holzforschung*, 1983, **37**, 55–61.
28 A. George, *et al.*, The effect of ionic liquid cation and anion combinations on the macromolecular structure of lignins, *Green Chem.*, 2011, **13**, 3375–3385.
29 M. Micic, *et al.*, Probing the lignin nanomechanical properties and lignin-lignin interactions using the atomic force microscopy, *Chem. Phys. Lett.*, 2001, **347**, 41–45.
30 T. K. Kirk, Biochemistry of lignin degradation by Phanerochaete chrysosporium, in *Biochemistry and genetics of cellulose degradation: Proceedings of the Federation of the Microbiological Societies symposium no. 43*, Academic Press inc., San Diego, CA, 1987, pp. 315–332.
31 Y.-R. Chen, S. Sarkanen and Y.-Y. Wang, Lignin-degrading enzyme activities, in *Biomass Conversion: Methods and Protocols*, ed. M. E. Himmel, Humana Press, 2012.
32 J. B. Binder, *et al.*, Reactions of lignin model compounds in ionic liquids, *Biomass Bioenergy*, 2009, **33**, 1122–1130.
33 S. Sarkanen, *et al.*, Associative interactions between kraft lignin components, *Macromolecules*, 1984, **17**, 2588–2597.
34 T. Saarinen, *et al.*, Adsorption of different laccases on cellulose and lignin surfaces, *BioResources*, 2009, **4**, 94–110.
35 D. Amarante, Applying *in situ* chemical oxidation, *Pollut. Eng.*, 2002, 40–42.
36 D. D. Gates-Anderson, R. L. Siegrist and S. R. Cline, Comparison of potassium permanganate and hydrogen peroxide as chemical oxidants for organically contaminated soils, *J. Environ. Eng.*, 2001, **127**, 337–347.
37 NAVFAC, In situ chemical oxidation of organic contaminants in soil and groundwater using Fenton's reagent, in *Tech Data Sheet*, 1999.

38 L. G. Covinich, *et al.*, Advanced oxidation processes for wastewater treatment in the pulp and paper industry: a review, *Am. J. Environ. Eng.*, 2014, **4**, 56–70.
39 G. Bentivenga, *et al.*, Degradation of steam-exploded lignin from beech by using Fenton's reagent, *Biomass Bioenergy*, 2003, **24**, 233–238.
40 K. Mae, *et al.*, A new conversion method for recovering valuable chemicals from oil palm shell wastes utilizing liquid-phase oxidation with HO under mild conditions, *Energy Fuels*, 2000, **14**, 1212–1218.
41 D. M. Kato, *et al.*, Pretreatment of lignocellulosic biomass using Fenton chemistry, *Bioresour. Technol.*, 2014, **162**, 273–278.
42 R. Bourbonnais, D. Leech and M. G. Paice, Electrochemical analysis of the interactions of laccase mediators with lignin model compounds, *Biochim. Biophys. Acta*, 1998, **1379**, 381–390.
43 P. J. Collins, A. D. W. Dobson and J. A. Field, Reduction of the 2,2′-azinobis(ethylbenzthiazoline-6-sulfonate) cation radical by physiological organic acids in the absence and presence of manganese, *Appl. Environ. Microbiol.*, 1998, **64**, 2026–2031.
44 C. Felby, J. Hassingboe and M. Lund, Pilot-scale production of fiberboards made by laccase oxidized wood fibers: board properties and evidence for cross-linking of lignin, *Enzyme Microb. Technol.*, 2002, **31**, 736–741.
45 G. Eligir, *et al.*, Laccase-initiated cross-linking of lignocellulose fibers using a ultra-filtered lignin isolated from kraft black liquor, *Appl. Microbiol. Biotechnol.*, 2007, **77**, 809–817.
46 K. Johansson, *et al.*, Comparison of lignin derivatives as substrates for laccase-catalyzed scavenging of oxygen in coatings and films, *J. Biol. Eng.*, 2014, **8**, 1.
47 R. Bourbonnais, *et al.*, Lignin oxidation by laccase isozymes from Trametes versicolor and role of the mediator 2,2′-azinobis(3-ethylbenzthiazoline-6-sulfonate) in kraft lignin depolymerization, *Appl. Environ. Microbiol.*, 1995, **61**, 1876–1800.
48 H. L. Hergert, *Infrared spectra, in Lignins - occurance, formation, structure and reactions*, ed. K. V. Sarkanen and C. H. Ludwig, Wiley-Intersci, New York, London, 1971, pp. 267–293.
49 Y. Z. Lai and K. V. Sarkanen, Structural variation in dehydrogenation polymers of coniferyl alcohol, *Cellul. Chem. Technol.*, 1975, **9**, 239–245.
50 O. Faix, Classification of lignins from different botanical origins by FT-IR spectroscopy, *Holzforschung*, 1991, **45**, 21–27.
51 C. Boeriu, *et al.*, Characterization of structure-dependent functional properties of lignin with infrared spectroscopy, *Ind. Crops Prod.*, 2004, **20**, 205–218.
52 O. Faix and O. Beinhoff, FTIR spectra of milled wood lignins and lignin polymer models (DHP's) with enhanced resolution obtained by deconvolution, *J. Wood Chem. Technol.*, 1988, **8**, 505–522.
53 K. K. Pandey and A. J. Pitman, FTIR studies of the changes in wood chemistry following decay by brown-rot and white-rot fungi, *Int. Biodeterior.Biodegrad.*, 2003, **52**, 151–160.
54 G. Hu, *et al.*, Structural characterization of switchgrass lignin after ethanol organosolv pretreatment, *Energy Fuels*, 2011, **26**, 740–745.
55 G. Milczarek, Preparation and characterization of a lignin modified electrode, *Electroanalysis*, 2007, **19**, 1411–1414.
56 F. Mijangos, F. Varona and N. Villota, Changes in solution color during phenol oxidation by Fenton reagent, *Environ. Sci. Technol.*, 2006, **40**, 5538–5543.
57 I. Dolamic and T. Burgi, Photocatalysis of dicarboxylic acids over TiO_2, An in situ ATR-IR study, *J. Catal.*, 2007, **248**, 268–276.
58 X. Pan, *et al.*, Biorefining of softwoods using ethanol organosolv pulping: preliminary evaluation of process streams for manufacture of fuel-grade ethanol and co-products, *Biotechnol. Bioeng.*, 2005, **90**, 473–481.
59 R. El Hage, *et al.*, Characterization of milled wood lignin and ethanol organosolv lignin from miscanthus, *Polym. Degrad. Stab.*, 2009, **94**, 1632–1638.
60 X. Pan, *et al.*, Bioconversion of hybrid poplar to ethanol and co-products using an organosolv fractionation process: optimization of process yields, *Biotechnol. Bioeng.*, 2006, **94**, 851–861.
61 L. A. Linden, *et al.*, Photooxidative degradation of polymers by hydroxyl and hydroperoxyl radicals generated during the photolysis of hydrogen peroxide, iron trichloride, and Fenton reagents, *Coord. Chem. Rev.*, 1993, **125**, 195–217.
62 A. R. Freitas, A. F. Rubira and E. C. Muniz, Degradation of polychloroprene/natural rubber (PCP/NR) blends by photo-Fenton process, *Polym. Degrad. Stab.*, 2008, **93**, 601–607.
63 N. Kang, D. S. Lee and J. Yoon, Kinetic modeling of Fenton oxidation of phenol and monochlorophenols, *Chemosphere*, 2002, **47**, 915–924.
64 R. Chen and J. Pignatello, Role of quinone intermediates as electron shuttles in Fenton and photoassisted Fenton oxidations of aromatic compounds, *Environ. Sci. Technol.*, 1997, **31**, 2399–2406.
65 J. A. S. Peres and L. H. Melo de Carvalho, Characteristics of p-hydroxybenzoic acid oxidation using Fenton's reagent, *J. Environ. Sci. Health, Part A*, 2004, **39**, 2897–2913.
66 C. K. Duesterberg, S. E. Mylon and T. D. Waite, pH effects on iron-catalyzed oxidation using Fenton's reagent, *Environ. Sci. Technol.*, 2008, **42**, 8522–8527.
67 Y.-H. Huang, *et al.*, Comparative study of oxidation of dye-Reactive Black B by different advanced oxidation processes: Fenton, electro-Fenton, and photo-Fenton, *J. Hazard. Mater.*, 2008, **154**, 655–662.
68 C. Ciotti, R. Baciocchi and T. Tuhkanen, Influence of the operating conditions on highly oxidative radicals generation in Fenton's systems, *J. Hazard. Mater.*, 2009, **161**, 402–408.
69 E. Araujo, *et al.*, Fenton's reagent - mediated degradation of residual Kraft black liquor, *Appl. Biochem. Biotechnol.*, 2002, **97**, 91–103.
70 J. Zeng, *et al.*, Biomimetic Fenton-catalysed lignin depolymerization to high-value aromatics and dicarboxylic acids, *ChemSusChem*, 2015, **8**, 861–871.

71 C. Walling, Fenton's reagent revisited, *Acc. Chem. Res.*, 1975, **8**, 125–131.
72 C. Walling, D. M. Camioni and S. S. Kim, Aromatic hydroxylation by peroxydisulfate, *J. Am. Chem. Soc.*, 1978, **100**, 4814–4818.
73 M. K. Eberhardt, Radiation-induced homolytic aromatic substitution. 6. The effect of metal ions on the hydroxylation of benzonitrile, anisole, and fluorobenzene, *J. Phys. Chem.*, 1977, **81**, 1051–1056.
74 G. W. Klein, *et al.*, Reaction of $^{\bullet}$OH with benzoic acid. Isomer distribution in the radical intermediates, *J. Phys. Chem.*, 1975, **79**, 1767–1774.
75 P. O'Neill, D. Schulte-Frohlinde and S. Steenken, Formation of radical cations and zwitterions versus demethoxylation in the reaction of OH with a series of methoxylated benzenes and benzoic acids, *Faraday Discuss. Chem. Soc.*, 1977, **63**, 141–148.
76 N. V. Raghavan and S. Steenken, Electrophilic reaction of the OH radical with phenol. Determination of the distribution of isomeric dihydroxycyclohexadienyl radicals, *J. Am. Chem. Soc.*, 1980, **102**, 3495–3499.
77 X. Fang, *et al.*, Reversibility in the reaction of cyclohexadienyl radicals with oxygen in aqueous solution, *Chem. – Eur. J.*, 1995, **1**, 423–429.
78 J. Gierer, Basic principles of bleaching. Part 1. Cationic and radical processes, *Holzforschung*, 1990, **44**, 387–394.
79 K. Tatsumi and N. Terashima, Cleavage of the β-O-4 linkage of guaiacylglycerol-β-guaiacyl ether by hydroxyl radicals, *Mokuzai Gakkaishi*, 1985, **31**, 316–317.
80 A. Aguiar and A. Ferraz, Fe^{3+} and Cu^{2+} -reduction by phenol derivatives associated with Azure B degradation in Fenton-like reactions, *Chemosphere*, 2007, **66**, 947–954.
81 V. Arantes, *et al.*, Effect of pH and oxalic acid on the reduction of Fe^{3+} by a biomimetic chelator and on Fe^{3+} desorption/adsorption onto wood: Implications for brown rot decay, *Int. Biodeterior. Biodegrad.*, 2009, **63**, 478–483.
82 Y. Sun and J. J. Pignatello, Chemical treatment of pesticide wastes. Evaluation of Fe(III) chelates for catalytic hydrogen peroxide oxidation of 2,4-D at circumneutral pH, *J. Agric. Food Chem.*, 1992, **40**, 322–327.
83 W. Varela and M. Tien, Effect of pH and oxalate on hydroquinone-derived hydroxyl radical formation during brown rot wood degradation, *Appl. Environ. Microbiol.*, 2003, **69**, 6025–6031.
84 C. Aulin, *et al.*, Nanoscale cellulose films with different crystallinities and mesostructures - Their surface properties and interaction with water, *Langmuir*, 2009, **25**, 7675–7685.
85 T. Tammelin, *et al.*, Preparation of lignin and extractive model surfaces by using spincoating technique - Application for QCM-D studies, *Nord. Pulp Pap. Res. J.*, 2006, **21**, 444–450.
86 A. Eudes, *et al.*, Production of hydroxycinnamoyl anthranilates from glucose in Escherichia coli, *Microb. Cell Fact.*, 2013, **12**(62), 1–10.
87 D. Juminaga, *et al.*, Modular engineering of L-tyrosine production in Escherichia coli, *Appl. Environ. Microbiol.*, 2012, **78**, 89–98.